An Enhanced Sensorless Control Scheme for PMSM Drives Considering Self-inductance Asymmetry

Lijian Wu, *Senior Member*, *IEEE*, Zekai Lyu, Zekai Chen, Jiaming Liu, and Ying Lu

***Abstract*—Inductance asymmetry, which is brought by inherent asymmetric parameters, manufacture tolerance, winding fault, cables with unequal lengths, etc., of permanent-magnet synchronous machines (PMSMs) can cause current harmonics and inaccurate position estimation. This paper proposes an enhanced fundamental model based sensorless control strategy for PMSMs with asymmetric inductances. The proportional-integral-resonant current regulator is introduced to reduce the second-order harmonics of currents, but there are still negative sequence components in the estimated back-electromotive forces (EMFs), which can cause the position estimated error. Differing from conventional methods in which negative sequences are filtered out before the phase-locked loop (PLL) module, the proposed method directly applies the estimated back-EMF with negative sequences as the reference input of PLL. An improved PLL with a bi-quad filter is proposed to attenuate the arising second harmonic position error and heighten the steady-state accuracy. Then, this position error is used for asymmetric inductance identification and its result is utilized to update the observer model. Furthermore, the dynamic performance is improved by the output limitation on the bi-quad filter as well as the implementation of a fast-locking technique in the PLL. The effectiveness of the proposed scheme is verified by experimental results.**

***Index Terms*—Inductance asymmetry, Permanent magnet synchronous machine (PMSM), Position estimation error, Sensorless control.**

I. INTRODUCTION

PERMANENT-magnet synchronous machines (PMSMs) are widely used in renewable energy generation and electrified transportation due to superior performances such as lower system cost, higher power density, and efficiency [1], [2]. The signals of speed and position obtained from encoders are needed in the field-oriented control of PMSMs. However, the existence of encoders increases the cost and volume of the machine drive system, and reduces reliability. Therefore, the investigation of sensorless control schemes for PMSMs has attracted wide attention recently [3], [4].

Various sensorless methods have been developed, which can be grouped into two categories. The first category is the machine-saliency-based sensorless control, which is generally realized through the high-frequency signal injection [5]-[9]. However, injected signals can produce more losses and larger torque ripples. The other category is the control based on the estimation of back-electromotive force (EMF) or flux linkage commonly exploited in the medium- and high-speed situations. This kind of method can be roughly categorized as: model reference adaptive system [10], extended Kalman filter [11], Luenberger observer[12], and sliding mode observer (SMO) [13], [14], etc. Among these methods, the SMO-based method is mainly investigated in this paper as it has good dynamic performance and robustness to disturbances.

The accuracy of estimated position and speed information, whatever steady-state or dynamic-state, can be affected by multifaceted factors, mainly including the accuracy of estimated back-EMFs [12]. The position estimation error is comprised of a dc offset and harmonic components. Some methods were developed to improve the accuracy of the sensorless control. In [15] the online parameter identification was applied to diminish the dc error caused by the parameter uncertainties. In [13], a quadrature phase-locked loop tracking estimator with an adaptive notch filter was proposed to reduce the position estimation harmonic error. Nevertheless, most researches are based on the healthy condition of PMSM, and the harmonic error caused by asymmetric machine parameters has not been fully considered. Meanwhile, in case of manufacture tolerance, winding fault, or single winding operation of dual three-phase PMSM, asymmetric inductance can appear and lead to the inaccuracy of estimated position information as the appearance of negative sequences of voltage and current, which was not considered in the symmetrical fundamental model. In [8], the influence of asymmetric machine resistances and self-inductances on carrier signal injection-based sensorless control has been investigated, which can be suppressed by the selection of injection frequency and the usage of dual-frequency injection. However, the influence of self-inductance asymmetry on EMF-based sensorless control has yet to be studied further.

In this paper, for PMSM with inductance asymmetry, an improved SMO-based sensorless control method is proposed to improve the steady-state and dynamic-state accuracy of position estimation. The proportional-integral-resonant (PIR)

Manuscript received November 11, 2022; accepted December 05, 2022. date of publication December 25, 2022; date of current version December 18, 2022.

This work was supported in part by the National Key R&D Program of China under Grant 2019YFB1503700, and in part by the National Natural Science Foundation of China under Grant 51977191. *(Corresponding author: Lijian Wu)*

L. Wu, Z. Lyu, and Z. Chen are with the College of Electrical Engineering, Zhejiang University, Hangzhou, 310027, China.(e-mail: ljw@zju.edu.cn; zklyu@zju.edu.cn; chenzk@zju.edu.cn)

J. Liu is with Shanghai Electric Wind Power Group Company, Ltd., Hangzhou, 310063, China.(e-mail: eliujiaming@hotmail.com)

Y. Lu is with the 21st Research Institute of China Electronics Technology Group Corporation, Ltd., Shanghai, 200030, China. (e-mail: 1825872894@qq.com)

Digital Object Identifier 10.30941/CESTEMS.2022.00050

regulator is applied to reduce the second harmonic errors of *d-q* axis currents. However, the negative sequences still exist in the estimated back-EMFs, which can lead to the inaccuracy of position and speed estimation. Differing from the conventional method in which current harmonics are filtered out before the PLL module, the proposed method directly takes the back-EMFs with negative sequences as the reference input of PLL. Besides, a bi-quad filter is incorporated in the PLL to attenuate the arising second harmonic position error and improve the steady-state accuracy. Moreover, this second harmonic error is used to identify the asymmetric inductance and the identification result is utilized to update the SMO sensorless model. Furthermore, the impact of the digital filter on the dynamic performance of PLL is analyzed, and the dynamic performance can be improved by the limitation on the filter output as well as the execution of a fast-locking technique (FLT) in the PLL. The effectiveness of the proposed method is verified on a 400-W surface-mounted PMSM test bench.

The contributions of this paper can be grouped into the following two categories. 1) The effects of self-inductance asymmetry on sensorless control of PMSM are investigated. A modified sensorless control scheme is proposed to diminish the position estimation error, which combines the improved PLL and asymmetric inductance identification. 2) The impact of the incorporated bi-quad filter on the dynamic performance of estimation is analyzed. On this base, the dynamic-state accuracy is improved by the execution of the FLT in the PLL as well as the limitation on the output of the digital filter. Moreover, this scheme can be extended to other back-EMF-based sensorless control to improve the dynamic performance.

II. Mathematical Model of PMSM With Three-Phase Self-Inductance Asymmetry

The voltage equations of the PMSM in the $\alpha\beta$-axis frame can be expressed as:

$$\begin{bmatrix} u_\alpha \\ u_\beta \end{bmatrix} = \begin{bmatrix} R_s & 0 \\ 0 & R_s \end{bmatrix} \begin{bmatrix} i_\alpha \\ i_\beta \end{bmatrix} + \begin{bmatrix} L_\alpha & L_{\alpha\beta} \\ L_{\alpha\beta} & L_\beta \end{bmatrix} p \begin{bmatrix} i_\alpha \\ i_\beta \end{bmatrix} + \begin{bmatrix} -\psi_f \omega_r \sin\theta_e \\ \psi_f \omega_r \cos\theta_e \end{bmatrix} \quad (1)$$

where p is the derivative operator; ψ_f represents the permanent magnet flux linkage; ω_r represents the electric angular velocity of the rotor; θ_e represents the electric angle of the rotor position; L_α, L_β, and $L_{\alpha\beta}$ represent transformed $\alpha\beta$-axis inductances, which could be presented as:

$$\begin{cases} L_\alpha = \dfrac{2}{3}L_A + \dfrac{1}{6}L_B + \dfrac{1}{6}L_C - M \\ L_\beta = \dfrac{1}{2}L_B + \dfrac{1}{2}L_C - M \\ L_{\alpha\beta} = \dfrac{\sqrt{3}}{6}L_C - \dfrac{\sqrt{3}}{6}L_B \end{cases} \quad (2)$$

where L_A, L_B, L_C, and M represent the three-phase self-inductances and mutual inductance, respectively. Then, the voltage equations in the dq-axis reference frame can be derived with the Park's transformation as follows:

$$\begin{bmatrix} u_d \\ u_q \end{bmatrix} = \begin{bmatrix} R_s & 0 \\ 0 & R_s \end{bmatrix} \begin{bmatrix} i_d \\ i_q \end{bmatrix} + \frac{\mathrm{d}}{\mathrm{d}t} \begin{bmatrix} \psi_d \\ \psi_q \end{bmatrix} + \begin{bmatrix} -\omega_r \psi_q \\ \omega_r \psi_d \end{bmatrix} \quad (3)$$

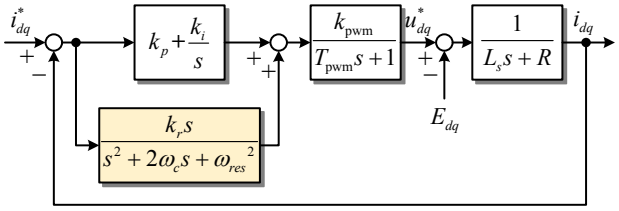

Fig. 1. Block diagram of current loop with PIR controller.

where the flux linkage equation of Ψ_{dq} is expressed as:

$$\begin{bmatrix} \psi_d \\ \psi_q \end{bmatrix} = \begin{bmatrix} \psi_f \\ 0 \end{bmatrix} + \begin{bmatrix} L_0 + L_2\cos 2\theta_e + L_{\alpha\beta}\sin 2\theta_e & -L_2\sin 2\theta_e + L_{\alpha\beta}\cos 2\theta_e \\ -L_2\sin 2\theta_e + L_{\alpha\beta}\cos 2\theta_e & L_0 - L_2\cos 2\theta_e - L_{\alpha\beta}\sin 2\theta_e \end{bmatrix} \begin{bmatrix} i_d \\ i_q \end{bmatrix} \quad (4)$$

where the dc and the second harmonic component of stator inductance in the dq-axis reference frame are obtained as:

$$\begin{cases} L_0 = \dfrac{1}{2}\left(L_\alpha + L_\beta\right) = \dfrac{1}{3}\left(L_A + L_B + L_C\right) - M \\ L_2 = \dfrac{1}{2}\left(L_\alpha - L_\beta\right) = \dfrac{1}{3}\left(L_A - \dfrac{1}{2}L_B - \dfrac{1}{2}L_C\right) \end{cases} \quad (5)$$

As can be seen from (5) that when one-phase self-inductance is unbalanced, in the dq reference frame, the inductance parameters contain the second harmonic components, leading to the second harmonic components of dq-axis currents when only proportional-integral (PI) controller is employed in the current control. Due to the second harmonic errors in the dq-axis currents, torque ripple and unstable speed arise consequently. Meanwhile, there are negative sequences in the estimated back-EMF, which can disturb the estimation of rotor position and speed.

III. Current Control and Enhanced Sliding-mode Sensorless Method

A. Current Control Using PIR Controller

In order to accurately track the harmonic components of current, the PIR controller is a commonly used method [16]-[18]. A PIR controller is realized by adding a resonant controller in parallel with the PI controller, as shown in Fig. 1. The transfer function of the resonant controller is designed as (6), which is the same as that of a second-order band pass filter (BPF):

$$G_r(s) = \frac{k_r s}{s^2 + 2\omega_c s + \omega_{res}^2} \quad (6)$$

where k_r is the gain of the controller, ω_c is the coefficient related to the bandwidth, and ω_{res} is the resonant frequency.

According to the transfer function, ω_{res} is the central frequency of the system, which guarantees the signal with corresponding frequency to pass the filter. k_r is a coefficient related to the dynamic response speed of the filter. In general, an ideal BPF only allowing the pass of signal with frequency ω_{res} is impractical, thus ω_c is set to widen the bandwidth of the resonant controller considering the sensitivity to the frequency scale of signals. According to [18], the resonant controller

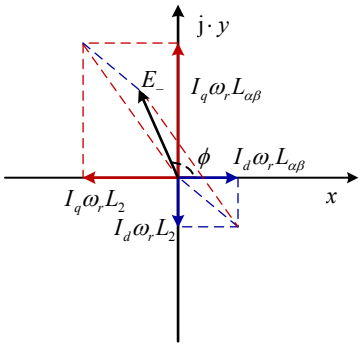

Fig. 2. The negative sequences of $\alpha\beta$-axis back-EMF in the form of space vector.

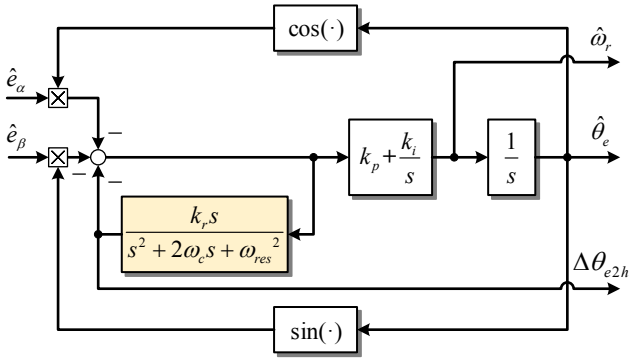

Fig. 3. Block diagram of PLL incorporated with the resonant controller.

makes sure the tracking of an AC component with no steady-state error. Hence, the second harmonic components in dq-axis currents can be accurately tracked through the resonant controller, ensuring the smooth control of current. It should be noted that the second harmonic components still exist in the dq-axis voltages at this moment.

However, as the second harmonic components exist in inductances, it can be derived from (4) and (5) that the second harmonic components of dq-axis flux linkage still exist, which lead to the second harmonic components of the estimated back-EMFs. The second harmonic components of back-EMFs in dq reference frame are equivalent to the negative sequences of $\alpha\beta$-axis back-EMFs, which can disturb the estimation of rotor position. The conventional idea is to filter out the negative sequences in the back-EMFs, e.g. using the synchronous reference frame filter (SRFF) [7]. In the proposed strategy of this paper, the basic idea is that the back-EMF with negative sequences is directly taken as the reference input of PLL. Besides, an improved PLL with a bi-quad filter is implemented by adding a resonant controller in it to filter the arising second harmonic position errors.

B. Improved PLL Incorporated with Digital Filter

Assuming that the dq-axis current is controlled smoothly, according to (3) and (4), the second harmonic components of voltages in the dq reference frame can be expressed by:

$$\begin{bmatrix} u_{d2h} \\ u_{q2h} \end{bmatrix} = \omega_r \begin{bmatrix} -L_2 \sin 2\theta_e + L_{\alpha\beta} \cos 2\theta_e & -L_2 \cos 2\theta_e - L_{\alpha\beta} \sin 2\theta_e \\ -L_2 \cos 2\theta_e - L_{\alpha\beta} \sin 2\theta_e & L_2 \sin 2\theta_e - L_{\alpha\beta} \cos 2\theta_e \end{bmatrix} \begin{bmatrix} I_d \\ I_q \end{bmatrix} \tag{7}$$

where I_d and I_q represent the fundamental component of dq-axis currents.

With the inverse Park's transformation, the negative sequences of estimated $\alpha\beta$-axis back-EMFs in the space vector form can be deduced as:

$$\begin{aligned} \vec{E}_{\alpha\beta-} &= I_d \omega_r \left(L_2 e^{\mathrm{j}(-\theta_e + 270^\circ)} + L_{\alpha\beta} e^{\mathrm{j}(-\theta_e)} \right) \\ &+ I_q \omega_r \left(L_2 e^{\mathrm{j}(-\theta_e + 180^\circ)} + L_{\alpha\beta} e^{\mathrm{j}(-\theta_e + 90^\circ)} \right) = E_- e^{\mathrm{j}(-\theta_e + \phi)} \end{aligned} \tag{8}$$

where E_- and Φ represent the amplitude and initial phase of the negative sequences, which is shown in Fig. 2.

Based on the analysis above, the estimated back-EMFs in the $\alpha\beta$-axis reference frame containing both the positive and negative sequences can be expressed simply by:

$$\begin{cases} e_\alpha = -E_+ \sin(\theta_e) - E_- \sin(-\theta_e + \phi) \\ e_\beta = E_+ \cos(\theta_e) + E_- \cos(-\theta_e + \phi) \end{cases} \tag{9}$$

Take the back-EMF from (9) as the reference input to the PLL, the error between the actual and estimated position can be obtained as:

$$\begin{aligned} \Delta\theta_e &= -e_\alpha \cos\hat{\theta}_e - e_\beta \sin\hat{\theta}_e \\ &= E_+ \sin(\theta_e - \hat{\theta}_e) + E_- \sin(-\theta_e - \hat{\theta}_e + \phi) \\ &\approx \underbrace{E_+(\theta_e - \hat{\theta}_e)}_{\text{DC term}} + \underbrace{E_- \sin(-\theta_e - \hat{\theta}_e + \phi)}_{\text{2nd harmonic term}} \end{aligned} \tag{10}$$

It can be found that the second harmonic position error arises. Only the dc component of position error is valid in the estimation of position, thus the second harmonic components should be reduced. In the proposed strategy, a resonant controller is implemented to extract the second harmonic components, and then it is fed back and subtracted from the position error, thus the dc component can be retained and then be used to estimate the rotor position. The block diagram of the proposed method is shown in Fig. 3.

The transfer function of the resonant controller written in (6) can be regarded as the feedback function of the closed loop. Thus, the closed-loop function of the section is derived as:

$$Z(s) = \frac{1}{1 + G_r(s)} = \frac{s^2 + 2\omega_c s + \omega_{res}^2}{s^2 + (2\omega_c + K_r)s + \omega_{res}^2} \tag{11}$$

The structure of proposed method is of the similar principle as the bi-quad filter. The signal with central frequency ω_{res} is constrained by the digital filter, thus the second harmonic position error can be filtered out when the central frequency ω_{res} is selected as $2\omega_r$. The transfer function of the bi-quad filter can be given as

$$G_b(s) = \frac{s^2 + k_2\omega_b s + \omega_b^2}{s^2 + k_1\omega_b s + \omega_b^2} \tag{12}$$

where ω_b is the notch frequency, k_1 and k_2 represent the filter coefficients. The -3 dB rejection bandwidth B_b and the bi-quad filter magnitude x_b at notch frequency can be expressed as

$$\begin{cases} B_b = k_1\omega_b \\ x_b = 20\lg(k_2/k_1) \end{cases} \tag{13}$$

Hence, the -3 dB rejection bandwidth B_r and magnitude x_r at central frequency of (11) can be derived as

$$\begin{cases} B_r = 2\omega_c + K_r \\ x_r = 20\lg\dfrac{2\omega_c}{2\omega_c + K_r} \end{cases} \tag{14}$$

From (14), it is known that the magnitude-frequency characteristic and phase-frequency characteristic of the proposed digital filter can be adjusted by the two parameters K_r and ω_c. It should be noted that unlike the conventional notch filter in which the signal with central frequency is just filtered out, the proposed digital filter extracts the second harmonic error and information within it can be made use of, which will be discussed in the next section.

IV. Accuracy Improvement

A. Parameter Selection and Output Limit of Resonant Controller

Although the bi-quad filter in the PLL compensates the second harmonic position error, its restriction to the signal with resonant frequency $2\omega_r$ can deteriorate the dynamic performance of the PLL. When a step input is applied to the reference speed or load torque of the system, the value of position error will deviate from zero, which can be regarded as the addition of an impulse-like signal to the steady-state position error, illustrated in Fig. 4. The digital filter restricts the pass of this impulse-like signal, as the component with resonant frequency $2\omega_r$ contained in the signal is also filtered out. From this perspective, the dynamic performance of the improved PLL decreases compared to the conventional PLL. More seriously, the risk of divergence might occur since the inaccurate estimated position and speed, caused by the poor dynamic performance of the PLL, are fed back to the control loop.

Appropriate parameters of the bi-quad filter should be chosen to make sure that the impulse-like signal can get through the filter as much as possible. The signal with resonant frequency contained in the impulse-like signal should not be filtered out quickly and in a large amount, thus the gain x_r of the digital filter should not be chosen too large. However, if x_r is chosen too small, the second harmonic position error cannot be compensated completely. Hence, the parameters of the filter in PLL can be tuned by comprehensively considering the stable operation of the system and the maximum deviation of the position error.

Although appropriate parameters of the bi-quad filter decrease the risk of divergence, the component with resonant frequency $2\omega_r$ contained in the impulse-like signal cannot be prevented from filtering. If the output of resonant controller just satisfies the compensation of the second harmonic position error, the impulse-like signal will not be restricted by the filter. Hence, the amplitude of resonant controller output should be limited to the steady-state level. In this solution, the amplitude is detected during the steady state, which will be used as the limited value of resonant controller output during the dynamic state. In practice, the threshold is broadened little more to ensure the tracking of the second harmonic position error. The position error when the resonant controller output limit is used or not and with different K_r during the dynamic is shown in

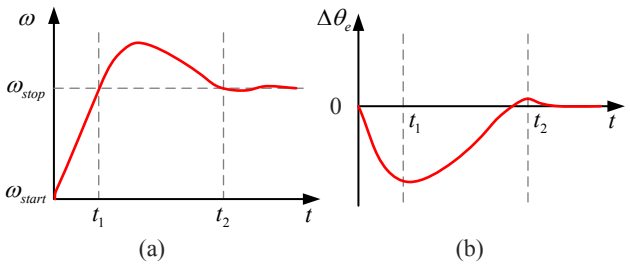

Fig. 4. Conceptual locking process of a conventional PLL with the dynamic stage of (a) estimated speed, and (b) position error.

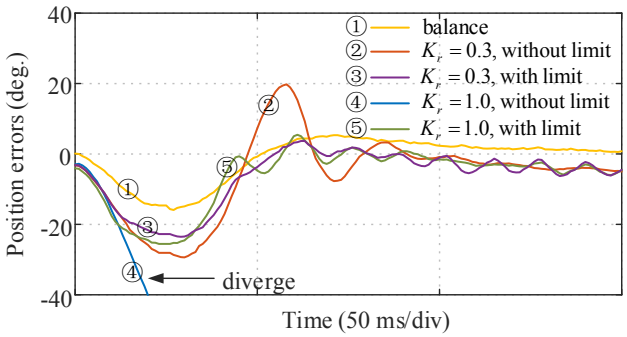

Fig. 5. Dynamic performance with different K_r and when the resonant controller output limit is used or not (1 N·m to 1.5 N·m at 0 s).

Fig. 5. It is shown that the proposed output limit can prevent the divergence and reduce the position error. It is noted that since the output limit constrains tracking of the second harmonic position error, there is a small amount of the position error in the dynamic state.

B. Fast-Locking Technique of PLL

As it is shown in Fig. 4, a speed error exists during the tracking process when a conventional PLL is used. As the position error is the integral value of speed error, it will deviate from zero, thus the estimated position is inaccurate during the dynamic state. Meanwhile, to track the actual position, the typical PLL must spend additional settling time to remove the integral value, as it is illustrated from t_1 to t_2 in Fig. 4, which can be solved to further improve the dynamic performance.

In [19], a fast-locking technique was proposed to solve the problem, which is introduced in this paper to improve the dynamic performance of PLL used in the SMO method. The conceptual locking process shown in Fig. 6 is demonstrated as follows: initially the accumulated position error implies that the actual position leads or lags the estimated one; then if the position error exceeds the set threshold, the estimated position is compensated to make it within the threshold, and the process will repeat until the estimated position tracks the actual one. The estimated speed should also be compensated to keep up with the change of estimated position. The position error when the FLT and the resonant controller output limit are used or not is shown in Fig. 7 (k_r = 0.3). As can be seen, the position error of the case with output limit and FLT remains within a threshold. Besides, the estimated position is approximately the same as the actual one during the dynamic state, and the tracking process is quicker.

In practice, the operation is more complicated since noise

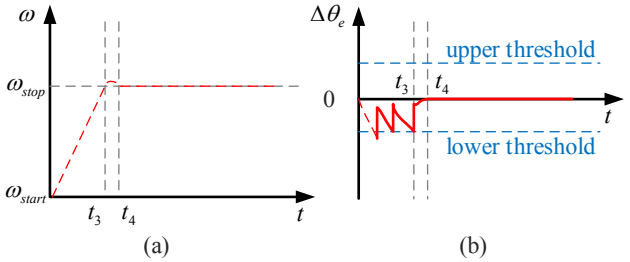

Fig. 6. Conceptual locking process of a PLL adopting the proposed FLT with the dynamic state of (a) estimated speed, and (b) position error.

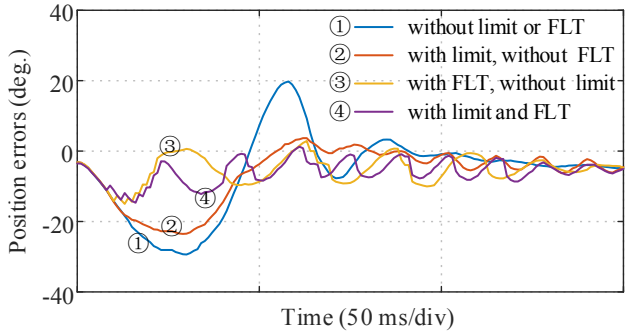

Fig. 7. Dynamic performance when the fast-locking technique and the resonant controller output limit are used or not (1 N·m to 1.5 N·m at 0 s).

exists in the position error which might cause the position error to exceed the set threshold and trigger an unnecessary compensation, shown in Fig. 8. As can be seen, the number of continuous periods where the error exceeds the threshold caused by a noise is limited, whereas the number caused by the deviation during the dynamic state is much larger.

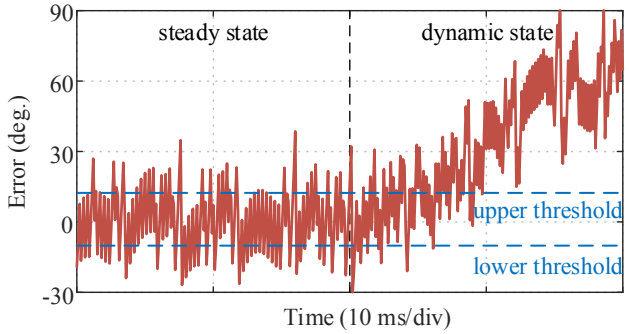

Fig. 8. The error fed back to the PLL with a noise.

In general, FLT can be regarded as a kind of discontinuous compensation, and it only works in the dynamic process. Based on the above analysis, only when the number of continuous periods in which the error exceeds the threshold meets a larger value, the compensation operation will be triggered. When the number of periods in which the error exceeds the threshold is less than the set threshold, it is judged as a false trigger and the FLT will not work.

C. Asymmetric Inductance Identification and SMO Model Update

The accuracy of inductance parameter in the SMO model has a significant influence on the accuracy of estimation. The asymmetric parameter can be identified from the second harmonic position error and be used to update the SMO model.

For $i_d = 0$ control strategy, as it is described in (8), the negative sequences of back-EMF in the $\alpha\beta$-axis reference frame can be expressed as:

$$\begin{aligned}\vec{E}_{\alpha\beta-} &= I_q\omega_r\left(L_2 e^{j(-\theta_e)} + L_{\alpha\beta}e^{j(-\theta_e+270^\circ)}\right)\\ &= E_{-}e^{j(-\theta_e+\phi)}\end{aligned} \tag{15}$$

where the amplitude E- can be expressed as:

$$\begin{aligned}E_{-} &= I_q\omega_r\sqrt{L_2{}^2 + L_{\alpha\beta}{}^2}\\ &= I_q\omega_r\sqrt{\left(\frac{1}{3}L_A-\frac{1}{6}L_B-\frac{1}{6}L_C\right)^2+\left(\frac{\sqrt{3}}{6}L_B-\frac{\sqrt{3}}{6}L_C\right)^2}\\ &= I_q\omega_r\sqrt{\left(\frac{1}{3}\Delta L_A-\frac{1}{6}\Delta L_B-\frac{1}{6}\Delta L_C\right)^2+\left(\frac{\sqrt{3}}{6}\Delta L_B-\frac{\sqrt{3}}{6}\Delta L_C\right)^2}\end{aligned} \tag{16}$$

where ΔL_A, ΔL_B and ΔL_C are asymmetric inductances of three phase, respectively.

It can be derived from (16) that the amplitude of negative sequences in the back-EMF is determined by the differences between three-phase asymmetric inductances. The amplitude of the second harmonic position error in (10) is the same as that of negative sequences, thus it contains the information related to three-phase self-inductances, which can be exploited to identify the asymmetric three-phase self-inductances.

To obtain the amplitude, a simple method is implemented based on the trigonometric function. Firstly, execute the integral operation on the extracted second harmonic position errors, a sine curve, to get a new sine curve lagging 90 electrical degrees. Then, for points with the same time on two curves, using the equation expressed in (17), the amplitude can be obtained.

$$\sqrt{\left(E_{-}\cos 2\theta_e\right)^2+\left(E_{-}\sin 2\theta_e\right)^2} = E_{-} \tag{17}$$

According to (4) and (5), the inductance parameter in the SMO model should be updated as follows:

$$\begin{aligned}L_{\text{updated}} &= L_0 = \frac{1}{3}\left(L_A+L_B+L_C\right)-M\\ &= L_{dq}+\frac{1}{3}\left(\Delta L_A+\Delta L_B+\Delta L_C\right)\end{aligned} \tag{18}$$

where L_{dq} represents the stator inductances in dq-axis frame.

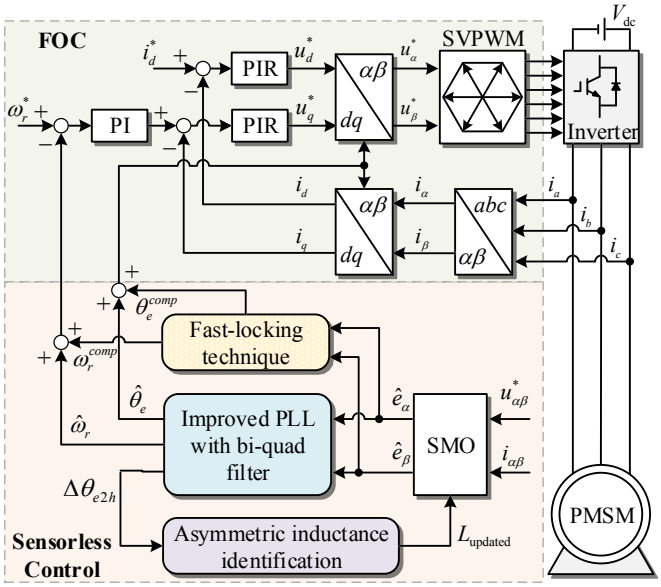

Fig. 9. Block diagram of overall control system.

In case when single-phase self-inductance is asymmetric, there is only one ΔL in (16) and (18). When I_q is not zero, the asymmetric self-inductance ΔL and updated inductance parameter in the SMO model can be obtained as:

$$\Delta L=\frac{3E_-}{\omega_r I_q} \tag{19}$$

$$L_{\text{updated}}=L_{dq}+\frac{\Delta L}{3} \tag{20}$$

The proposed identification method is simple to utilize compared to other methods, such as the signal-injection method [5] and recursive least square (RLS) method [15]. Then the overall control diagram of the proposed sensorless PMSM drives considering self-inductance asymmetry is shown in Fig. 9, including the improved PLL with bi-quad filter, FLT, and asymmetric inductance identification.

V. Experimental Validation

The proposed method is implemented on a dSPACE platform. The overall test setup is shown in Fig. 10, in which two surface-mounted PMSMs are used as the test and the load, respectively. The detailed parameters of the machine are given in Table I. The inductance asymmetry condition is created by connecting an extra inductor of 5 mH in series to the phase-A of the test machine. The switching frequency of inverter is set as 10 kHz. All the following experimental waveforms were achieved with the test PMSM operating at sensorless control. The actual rotor position is measured by an incremental encoder and used for evaluating the position estimation accuracy.

TABLE I
PMSM Parameters

Parameter	Value	Parameter	Value
Rated power (W)	400	Pole pairs	4
Rated speed (r/min)	3000	Stator inductance L_{dq} (mH)	6.65
Rated current (A)	2.7	Stator resistance R_s (Ω)	2.35
Rated torque (N·m)	1.27	Rotor flux linkage ψ_f (Wb)	0.062

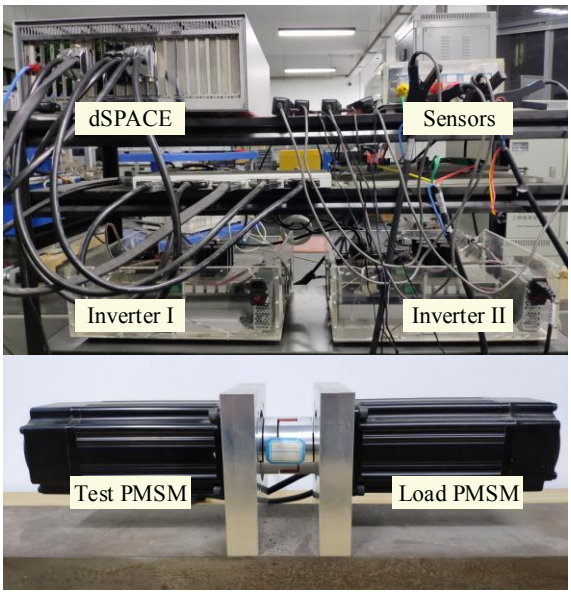

Fig. 10. Experimental setup.

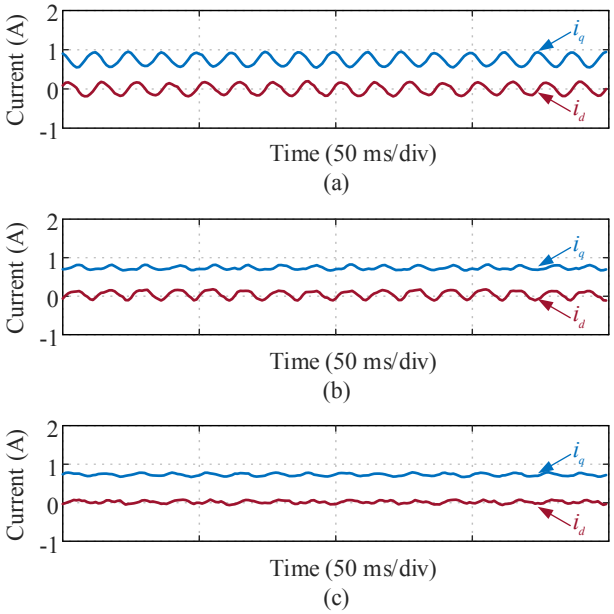

Fig. 11. *dq*-axis currents (a) without extra algorithm, (b) with PIR current control and without proposed sensorless method, and (c) with PIR current control and with proposed sensorless method.

Fig. 11 shows the current comparison at 600 r/min with 25% rated load. Fig. 11 (a) shows that the second harmonic current components are obvious under the condition without extra algorithm. Fig. 11 (b) shows that the execution of PIR controller in the current control can partially reduce the second harmonic components. Fig. 11 (c) illustrates that the proposed sensorless control scheme can further suppress the second harmonic current components caused by the estimated position error, which is beneficial to the reduction of torque ripple and power loss.

Fig. 12 shows the position estimation errors at 600 r/min with 25% rated load. Fig. 12 (a) shows the experimental result without extra algorithm, and Fig. 12 (b) shows the experimental result only with PIR current control. It can be seen that and the rotor position estimation error is reduced since the PIR current controller decreases the second harmonic components of the current. However, as aforementioned, due to the presence of the second harmonic caused by the harmonic component of the *dq*-axis flux linkage in the back-EMF, there is still a large error in the estimated rotor position. This harmonic position error can be obviously reduced with the proposed sensorless control, shown in Fig. 12 (c).

The harmonic spectrum of above position errors is shown in Fig. 13. Owing to the PIR current control and improved PLL, the amplitude of the second harmonic has been significantly reduced. However, the position estimation has a steady error as the result of inaccurate inductance, as shown in Fig. 12 (c), which can be compensated with the asymmetry identification in the proposed scheme. The value of identified asymmetric inductance is shown in Fig. 14, which fluctuates around the actual value of 5 mH. Fig. 12 (d) shows the experimental results with asymmetric inductance compensation. It can be concluded that the proposed sensorless control scheme can reduce the second harmonic position error as well as the steady position error in the steady state.

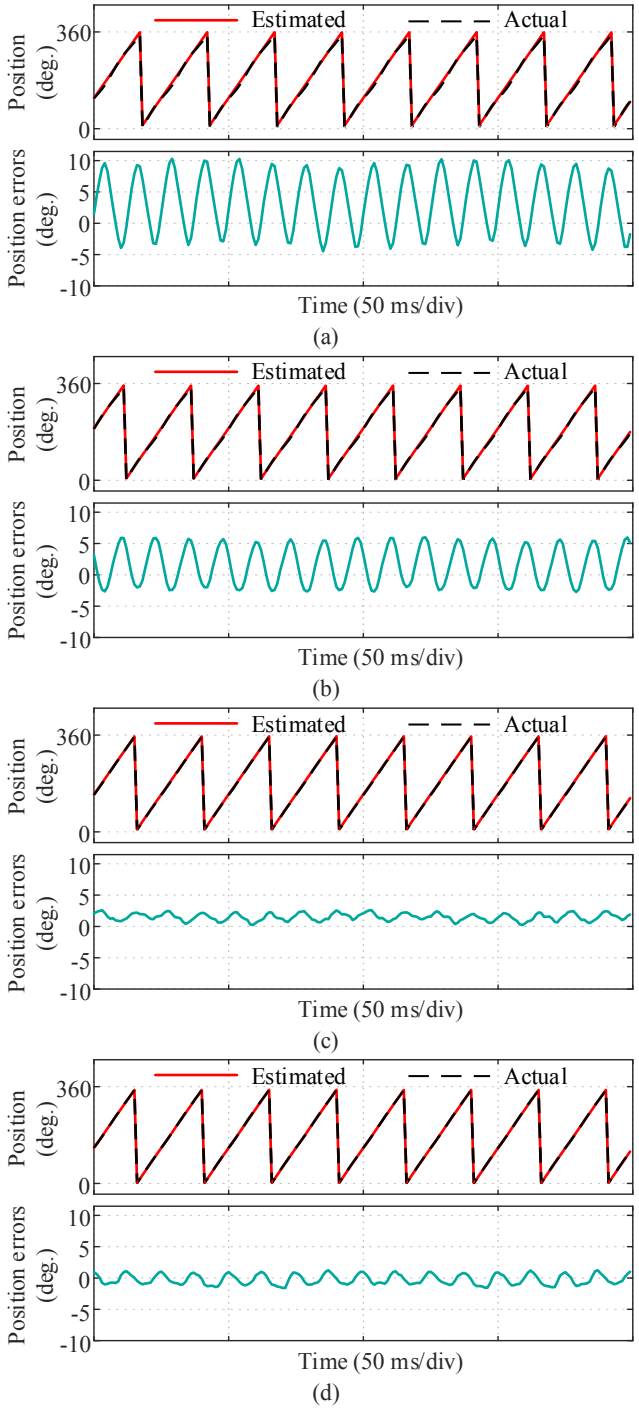

Fig. 12. Rotor position estimation at steady-state, 600r/min, (a) without extra algorithm, (b) with PIR current control and without proposed sensorless method, (c) with PIR current control and with proposed sensorless method, and (d) with asymmetric inductance compensation.

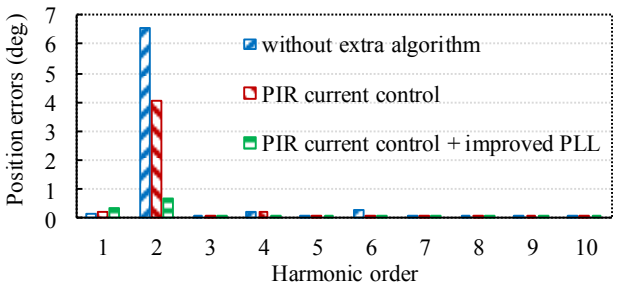

Fig. 13. Harmonic spectrum of position errors.

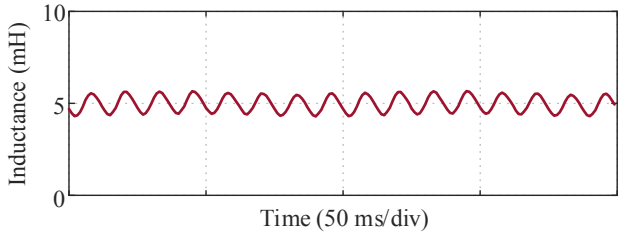

Fig. 14. Asymmetric inductance identification.

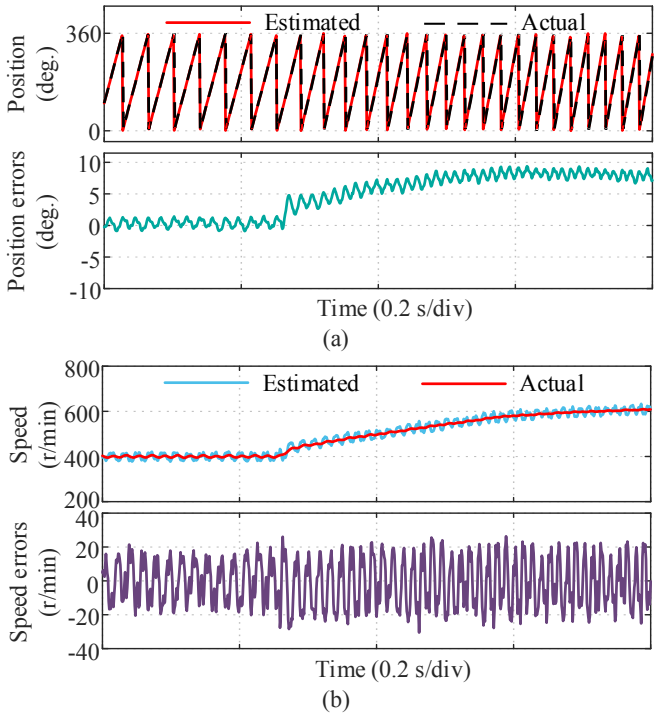

Fig. 15. Rotor position estimation without fast-locking technique under step speed condition. (a) Rotor positions and error. (b) Speed response.

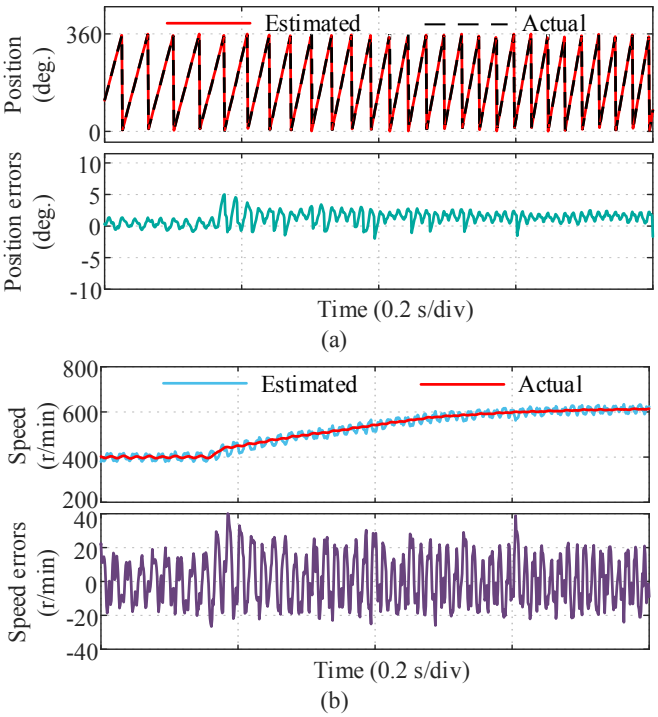

Fig. 16. Rotor position estimation with fast-locking technique under step speed condition. (a) Rotor positions and error. (b) Speed response.

Fig. 15 and Fig. 16 show the position and speed estimation errors under step speed condition from 400 r/min to 600 r/min with 25% rated load. It is illustrated from Fig. 15 (a) that the position error deviates from zero in the dynamic state without FLT. Comparatively, it can be seen from Fig. 16 (a) that the tracking accuracy has been improved with the FLT used in the proposed method. However, the estimated speed shown in Fig. 16 (b) has a relatively larger fluctuation during the dynamic procedure due to the speed compensation of FLT, but it is still within an acceptable range.

Besides, the effectiveness of the proposed sensroless control scheme is also validated with step load disturbance at 600 r/min, as shown in Fig. 17. The position estimation errors when decreasing and increasing the load are within 4.0° and 5.6°, respectively.

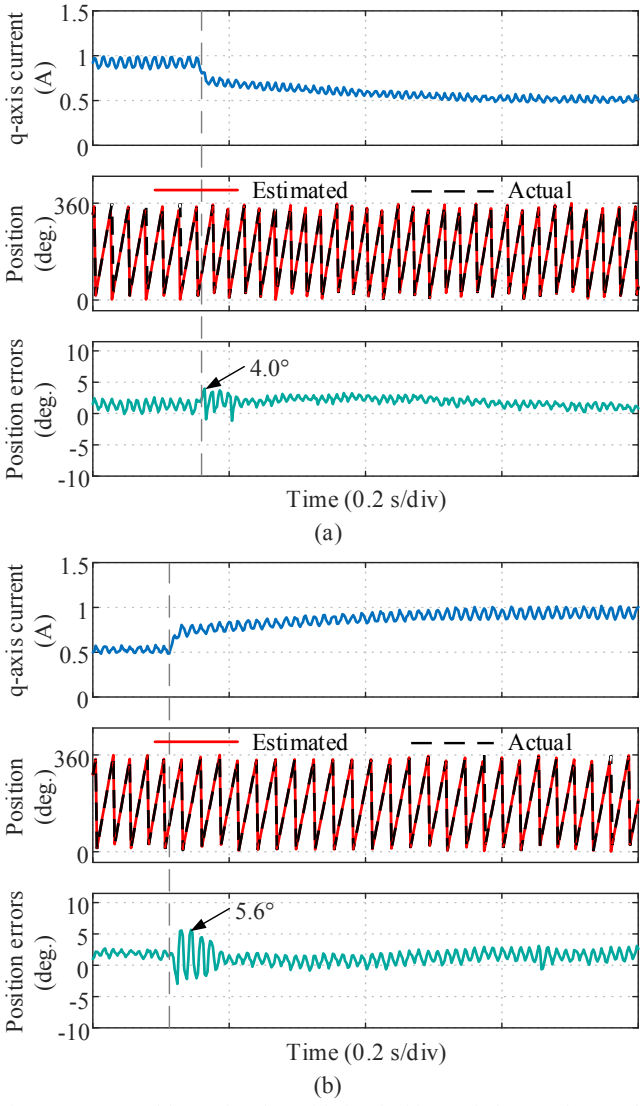

Fig.17. Rotor position estimation with fast-locking technique under step load condition, 600 r/min. (a) Load decrease. (b) Load increase.

VI. Conclusion

This paper presents an enhanced sensorless control strategy for PMSM considering self-inductance asymmetry, which can improve the position estimation accuracy in both steady and transient states. The influence of the asymmetric machine self-inductances is fully investigated and it can be concluded that the asymmetric situation causes second harmonic and dc offset error in position estimation, and also affects current control. The PIR current controller can decrease the second harmonic components of the current. Besides, the proposed PLL incorporated with a bi-quad filter has obviously reduced the arising second harmonic position error, and the second harmonic components of currents have been further attenuated with the improved estimated position. Meanwhile, the extracted second harmonic position error has been used for asymmetric inductance identification, which has been utilized to compensate the dc offset error of position estimation. Furthermore, to suppress the adverse impacts of the digital filter in the PLL, the fast-locking architecture combining output limit and discontinuous compensation has been introduced to further improve the dynamic-state accuracy of position estimation. Finally, the effectiveness and feasibility of the proposed strategy are verified at a 400-W PMSM sensorless drive.

References

[1] Z. Q. Zhu and D. Howe, "Electrical machines and drives for electric, hybrid, and fuel cell vehicles," *Proc. IEEE*, vol. 95, no. 4, pp. 746-765, Apr. 2007.

[2] K. T. Chau, C. C. Chan and C. Liu, "Overview of permanent-magnet brushless drives for electric and hybrid electric vehicles," *IEEE Trans. Ind. Electron.*, vol. 55, no. 6, pp. 2246-2257, Jun. 2008.

[3] G. Wang, M. Valla and J. Solsona, "Position sensorless permanent magnet synchronous machine drives—a review," *IEEE Trans. Ind. Electron.*, vol. 67, no. 7, pp. 5830-5842, Jul. 2020.

[4] D. Xu, B. Wang, G. Zhang, G. Wang and Y. Yu, "A review of sensorless control methods for AC motor drives," *CES Trans. Elect. Mach. Syst.*, vol. 2, no. 1, pp. 104-115, Mar. 2018.

[5] S. Morimoto, M. Sanada and Y. Takeda, "Mechanical sensorless drives of IPMSM with online parameter identification," *IEEE Trans. Ind. Appl.*, vol. 42, no. 5, pp. 1241-1248, Sep.-Oct. 2006

[6] Y. Yoon, S. Sul, S. Morimoto and K. Ide, "High-bandwidth sensorless algorithm for AC machines based on square-wave-type voltage injection," *IEEE Trans. Ind. Appl.*, vol. 47, no. 3, pp. 1361-1370, May-Jun. 2011.

[7] J. M. Liu and Z. Q. Zhu, "Novel sensorless control strategy with injection of high-frequency pulsating carrier signal into stationary reference frame," *IEEE Trans. Ind. Appl.*, vol. 50, no. 4, pp. 2574-2583, Jul.-Aug. 2014.

[8] P. L. Xu and Z. Q. Zhu, "Carrier signal injection-based sensorless control for permanent-magnet synchronous machine drives considering machine parameter asymmetry," *IEEE Trans. Ind. Electron.*, vol. 63, no. 5, pp. 2813-2824, May 2016.

[9] G. Zhang, G. Wang, B. Yuan, R. Liu and D. Xu, "Active disturbance rejection control strategy for signal injection-based sensorless IPMSM drives," *IEEE Tran. Transport. Electrific.*, vol. 4, no. 1, pp. 330-339, Mar. 2018.

[10] A. Piippo, M. Hinkkanen and J. Luomi, "Analysis of an adaptive observer for sensorless control of interior permanent magnet synchronous motors," *IEEE Trans. Ind. Electron.*, vol. 55, no. 2, pp. 570-576, Feb. 2008.

[11] S. Bolognani, L. Tubiana and M. Zigliotto, "Extended kalman filter tuning in sensorless PMSM drives," *IEEE Trans. Ind. Appl.*, vol. 39, no. 6, pp. 1741-1747, Nov.-Dec. 2003.

[12] S. Bolognani, S. Calligaro and R. Petrella, "Design issues and estimation errors analysis of back-EMF-based position and speed observer for SPM synchronous motors," *IEEE J. Emerg. Sel. Topics Power Electron.*, vol. 2, no. 2, pp. 159-170, Jun. 2014.

[13] G. Wang, H. Zhan, G. Zhang, X. Gui and D. Xu, "Adaptive compensation method of position estimation harmonic error for EMF-based observer in sensorless IPMSM drives," *IEEE Trans. Power Electron.*, vol. 29, no. 6,

pp. 3055-3064, Jun. 2014.

[14] D. Liang, J. Li and R. Qu, "Sensorless control of permanent magnet synchronous machine based on second-order sliding-mode observer with online resistance estimation," *IEEE Trans. Ind. Appl.*, vol. 53, no. 4, pp. 3672-3682, Jul.-Aug. 2017.

[15] Y. Inoue, K. Yamada, S. Morimoto and M. Sanada, "Effectiveness of voltage error compensation and parameter identification for model-based sensorless control of IPMSM," *IEEE Trans. Ind. Appl.*, vol. 45, no. 1, pp. 213-221, Jan.-Feb. 2009.

[16] J. Hu, Y. He, L. Xu and B. W. Williams, "Improved control of DFIG systems during network unbalance using PI–R current regulators," *IEEE Trans. Ind. Electron.*, vol. 56, no. 2, pp. 439-451, Feb. 2009.

[17] C. A. Busada, S. Gomez Jorge, A. E. Leon and J. A. Solsona, "Current controller based on reduced order generalized integrators for distributed generation systems," *IEEE Trans. Ind. Electron.*, vol. 59, no. 7, pp. 2898-2909, Jul. 2012.

[18] C. Xia, B. Ji and Y. Yan, "Smooth speed control for low-speed high-torque permanent-magnet synchronous motor using proportional-integral-resonant controller," *IEEE Trans. Ind. Electron.*, vol. 62, no. 4, pp. 2123-2134, Apr. 2015.

[19] W. Chiu, Y. Huang and T. Lin, "A dynamic phase error compensation technique for fast-locking phase-locked loops," *IEEE J. Solid-State Circuits*, vol. 45, no. 6, pp. 1137-1149, Jun. 2010.

Lijian Wu (M'11-SM'14) received the B.Eng. and M.Sc. degrees from Hefei University of Technology, Hefei, China, in 2001 and 2004, respectively, and the Ph.D. degree from the University of Sheffield, Sheffield, U.K., in 2011, all in electrical engineering.

From 2004 to 2007, he was an Engineer with Delta Electronics (Shanghai) Co, Ltd. From 2012 to 2013, he was with Sheffield Siemens Wind Power Research Center as a design engineer focusing on wind power generators. From 2013 to 2016, he was an advanced engineer with Siemens Wind Power A/S, Brande, Denmark. Since 2016, he has been with Zhejiang University, where he is currently Professor of electrical machines and control systems. His current major research interests include design and control of permanent magnet machines.

Zekai Lyu (S'21) received the B.Eng. degree from Southwest Jiaotong University, Chengdu, China, in 2018, and the M.Sc. degree from Harbin Institute of Technology, Harbin, China, in 2020, both in electrical engineering. He is currently working toward the Ph.D. degree in electrical engineering with Zhejiang University, Hangzhou, China.

His current research interests include wide-bandgap device applications and electrical machine drives.

Zekai Chen received the B.Eng. and M.Sc. degrees in electrical engineering from Zhejiang University, Hangzhou, China, in 2018 and 2021, respectively.

His research interests include control of permanent magnet synchronous motors.

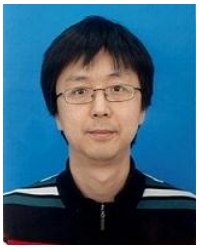

Jiaming Liu (M'13) received the B.Sc. and M.Sc. degrees in electrical engineering from Tianjin University, Tianjin, China, in 2007 and Zhejiang University, Hangzhou, China, in 2010, respectively, and the Ph.D. degree from The University of Sheffield, Sheffield, U.K., in 2013.

In 2010, he was an Electrical Engineer with Delta Electronic (Shanghai) Co., Ltd. From 2013 to 2019, he was Development Engineer with Siemens Wind Power Plc, Keele, U.K. He is currently with Shanghai Electric Wind Power Group Co., Ltd., China. His research interests include wind power converter and control of permanent-magnet wind-power generators.

Ying Lu received the B.Eng. degrees in electrical engineering from Hefei University of Technology, Hefei, China, in 1998.

She is currently a Senior Engineer with the 21st Research Institute of China Electronics Technology Group Corporation, Ltd., Shanghai, China. Her current research focuses on DC servo motors and special machines.